A New Compound-Limbs Paradigm: Integrating Upper-Limb Swing Improves Lower-Limb Stepping Intention Decoding From EEG

Rui Ma, Yi-Feng Chen, *Member, IEEE*, Yi-Chuan Jiang, *Graduate Student Member, IEEE*, and Mingming Zhang, *Senior Member, IEEE*

***Abstract*— Brain-computer interface (BCI) systems based on spontaneous electroencephalography (EEG) hold the promise to implement human voluntary control of lower-extremity powered exoskeletons. However, current EEG-BCI paradigms do not consider the cooperation of upper and lower limbs during walking, which is inconsistent with natural human stepping patterns. To deal with this problem, this study proposed a stepping-matched human EEG-BCI paradigm that involved actions of both unilateral lower and contralateral upper limbs (also referred to as compound-limbs movement). Experiments were conducted in motor execution (ME) and motor imagery (MI) conditions to validate the feasibility. Common spatial pattern (CSP) proposed subject-specific CSP (SSCSP), and filter-bank CSP (FBCSP) methods were applied for feature extraction, respectively. The best average classification results based on SSCSP indicated that the accuracies of compound-limbs paradigms in ME and MI conditions achieved 89.02% ± 12.84% and 73.70% ± 12.47%, respectively. Although they were 2.03% and 5.68% lower than those of the single-upper-limb mode that does not match human stepping patterns, they were 24.30% and 11.02% higher than those of the single-lower-limb mode. These findings indicated that the proposed compound-limbs EEG-BCI paradigm is feasible for decoding human stepping intention and thus provides a potential way for natural human control of walking assistance devices.**

***Index Terms*— Compound limbs, EEG, human stepping intention, motor imagery, motor execution.**

Manuscript received 12 January 2023; revised 19 May 2023 and 16 July 2023; accepted 8 September 2023. Date of publication 15 September 2023; date of current version 3 October 2023. This work was supported in part by the National Natural Science Foundation of China under Grant 62273173; in part by the Shenzhen Science and Technology Program under Grant JCYJ20220530113811027, Grant JCYJ20220818103602004, and Grant JCYJ20210324104203010; in part by the Shenzhen Key Laboratory of Smart Healthcare Engineering under Grant ZDSYS20200811144003009; in part by the National Key Research and Development Program of China under Grant 2022YFF1202500 and Grant 2022YFF1202502; in part by the Guangdong Provincial Key Laboratory of Advanced Biomaterials under Grant 2022B1212010003; and in part by the Research Program of Guangdong Province under Grant 2020ZDZX3001 and Grant 2019ZT08Y191. *(Rui Ma and Yi-Feng Chen are co-first authors.) (Corresponding author: Mingming Zhang.)*

This work involved human subjects or animals in its research. Approval of all ethical and experimental procedures and protocols was granted by the Human Participant Ethics Committee of the Southern University of Science and Technology under Application No. 20210024.

The authors are with the Shenzhen Key Laboratory of Smart Healthcare Engineering and Guangdong Provincial Key Laboratory of Advanced Biomaterials, Department of Biomedical Engineering, Southern University of Science and Technology, Nanshan, Shenzhen 518055, China (e-mail: mar3@mail.sustech.edu.cn; chenyf6@sustech.edu.cn; 12031322@mail.sustech.edu.cn; zhangmm@sustech.edu.cn).

This article has supplementary downloadable material available at https://doi.org/10.1109/TNSRE.2023.3315717, provided by the authors.

Digital Object Identifier 10.1109/TNSRE.2023.3315717

I. Introduction

BRAIN-COMPUTER interface (BCI) system detects, analyzes, and converts brain signals to commands for controlling external devices [1]. Different techniques have been used to measure brain signals for BCIs. Electroencephalography (EEG) is one of such methods and has been widely applied because of its non-invasiveness, portability, and high temporal resolution [2]. In general, there are four basic rhythms in EEG, mainly including delta (0-4 Hz), theta (4-7 Hz), alpha (8-13 Hz), and beta (13-30 Hz) rhythms [3]. Specially, brain waves over the motor cortex in the band of (8-12 Hz) are also referred to as the mu rhythm [3]. As spatiotemporal amplitudes of mu and beta rhythms are modulated differently by moving different body parts, thus movement of specific limbs can normally be classified by analyzing the EEG rhythms [4]. Then the output of classification is converted into commands for an external device.

Motor imagery (MI) is one of the most investigated BCI paradigms. In this paradigm, participants perform imagery of moving different body parts (e.g. left hand, right hand, tongue, and foot) without actually moving or muscle contraction [5]. Compared to motor execution (ME) which involves actual movement, MI also can induce similar EEG rhythms [6]. Currently, one of the most important BCI applications is leveraging MI information to control walking-assisted exoskeletons that enable paralyzed patients to perform walking training with their proactive intentions [7], [8]. However, it should be noted that most BCI-MI paradigms lack the naturality to meet people's daily interaction habits, which might reduce comfort and effectiveness in practical applications. An intuitive and natural MI process, i.e.,

matching the way how human limbs naturally move [9], might be beneficial for promoting practical applications of BCI systems [10], [11].

Previous studies involving human walking MI-BCI can be generally divided into three types. The first type is imagining the start or stop of walking to activate or halt lower-limb rehabilitation exoskeletons [12]. While the start and stop of human walking have been recognized with acceptable average accuracy, i.e., 78.96% in [12], 81.81% in [13], and 83.5% in [14], this paradigm did not take the unilateral discrimination of the legs into account. As for the second type, most studies have applied MI of the left hand, the right hand, and both feet to achieve multi-command decoding. For example, Lee et al. [15] instructed human subjects to imagine moving both hands, the left hand and right hand, mapping intentions of walking forward, turning left, and turning right, respectively, in which the overall accuracy was 91%. Gao et al. [16] applied MI of the left hand, the right hand, and both feet to reflect intentions of ascending stairs, descending stairs, and walking, respectively. Wang et al. [17] utilized the same imagined actions as in [15] to represent intentions of sitting down, standing up, and walking, respectively. Their best classification accuracy was 85.33%. However, walking is a movement that related to lower limbs. This type of paradigm is not a direct and natural way to reflect the human walking process.

The third type is imagining the specific action process of lower limbs, which is closer to walking movement. The state-of-the-art literature about this type can be further generalized into two major categories: 1) imagine the dorsiflexion or/and plantarflexion of feet; 2) imagine the extension or/and flexion of thighs and calves. In the first category, Hashimoto and Ushiba [18] analyzed the MI features of left- and right-foot dorsiflexion. Their results suggested that there was potential to differentiate the left and right foot MI via the beta rebound, with an average accuracy of 69.3%. Tariq et al. [19] suggested that the best average accuracy was observed for beta ERS, given as 74.9%. Gu et al. [20] used a similar MI paradigm of feet and graph theory features were exerted to find out the difference in cortical signal characteristics. Their classification accuracy averaged 67.13%. For the second category (left- and right-leg MI), Hsu et al. [21] implemented a lower-limb MI paradigm in which human participants lifted their left or right legs on a step tool. Their results indicated that the mu rhythm contributed more to the higher classification accuracy (71.25%). Similar research was conducted by Liu et al. [22], but it was found that there exhibited no distinct event-related desynchronization/synchronization (ERD/ERS) difference between the MI of the left and right leg. The classification results were not provided. Kline et al. [23] developed an fMRI-informed EEG approach to enable an accurate mapping of spatial brain activity corresponding to the EEG electrodes, thereby improving the accuracy of lower-limb MI-BCI. Their average classification accuracy achieved 66.5%. A recent study guided participants to lie down on a specially-designed device [24], where they imagined leg flexion and extension processes of their legs. The average accuracy of this paradigm was 59.75%.

Compared with upper-limb paradigms, the classification accuracies of lower-limb MI paradigms were lower. There are two possible reasons: 1) the positions of the motor cortex controlling the movement of lower limbs are deeper and smaller (medial surface of the motor strip in the interhemispheric fissure) than those of upper limbs, which results in a minor spatial distance between the cortex areas corresponding to the left and right lower limb movements; 2) EEG does not have enough spatial resolution to probe the brain activity about 5cm perpendicular to the human scalp [25]. Therefore, it could be hypothesized that a paradigm that integrates actions of both upper and lower limbs might benefit to improve the classification accuracy. Because this paradigm could leverage the significant unilateral activation characteristics of upper limbs. Besides, since natural human walking is a coordinated movement involving both upper and lower limbs, the participation of upper limbs should not be ignored while designing the natural human walking MI-BCI.

Several recent studies have considered investigating the brain response to multi-limbs tasks. Yi et al. implemented a series of studies [26], [27], [28] to explore characteristics of hand-foot combination tasks. These tasks were the imitation of playing drums by single-hand or compound actions of the unilateral hand and the contralateral foot. Their findings indicated the imagination of one hand and one foot contributed to the simultaneous activation of contralateral and mid-central brain areas. Besides, Weersink et al. [29], [30] suggested that there was stronger ERD when humans walked accompanied by natural arm swing than that of without-arm swing in the supplementary motor area (SMA). These findings provide a feasibility foundation for investigating the compound-limbs paradigm.

In our preliminary study [31], we designed an arm-leg combination ME paradigm to investigate the characteristics of compound-limbs tasks on five subjects. In this work, we (1) extended the participants of the ME experiment and provided a more thorough feature and classification analysis, and (2) expanded the EEG-based compound-limbs paradigm to the MI condition. This compound-limbs paradigm involved the execution/imagination of stepping forward the unilateral lower limb alternatively and swinging forward the contralateral upper limb simultaneously. The main contributions of this study are as follows: 1) a new EEG-BCI paradigm of compound-limbs tasks integrating upper-limb swing and lower-limb stepping has been proposed; 2) the effect of compound-limbs tasks on the cerebral cortex is illustrated in terms of the time-frequency analysis of EEG; 3) extensive experiments were conducted on two representative EEG-based BCI conditions, namely motor execution and motor imagery, to verify the feasibility of the proposed paradigm. It is hoped that this work will promote the practical application of natural human stepping MI-BCI in the field of lower-extremity exoskeletons.

II. Methods

This section includes five parts. Parts A and B involve the introduction of the experiment protocol, data collection, and processing. The methods of feature extraction and classifiers were depicted in part C. The analytical methods

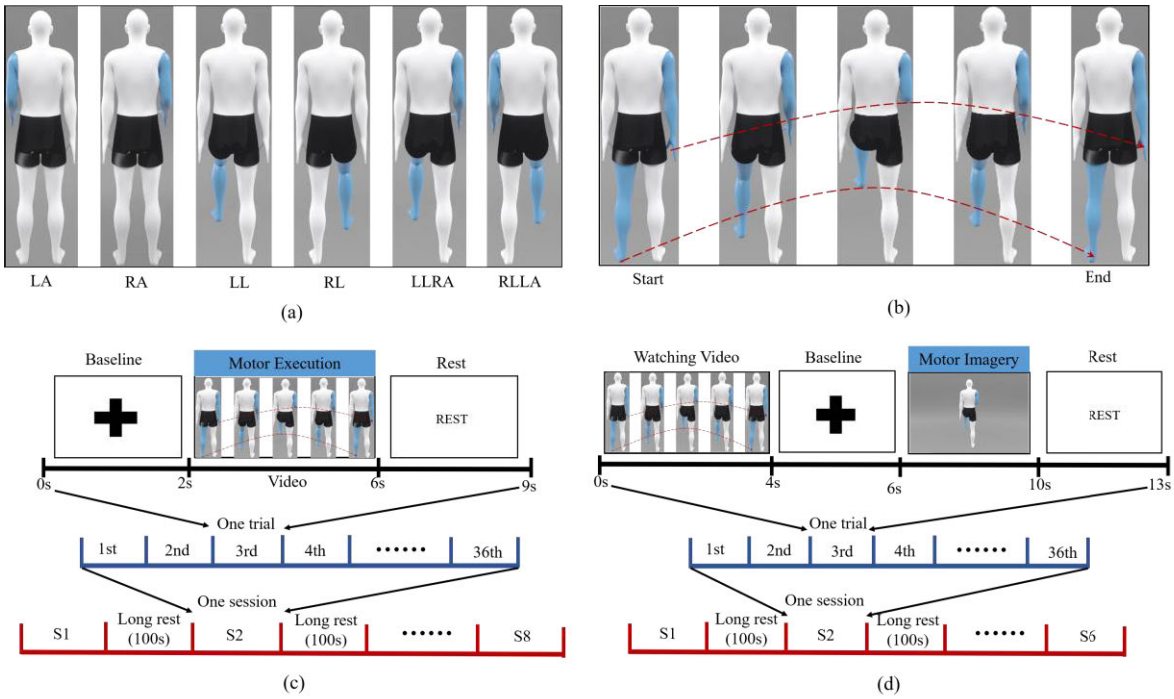

Fig. 1. Experiment protocol. (a): The design of single-limb and compound-limbs tasks.; (b): The action process shown in the video, tasking the LLRA task as example; (c) (d): The paradigm timeline of motor execution and motor imagery respectively. Abbreviation notes: LA: left arm; RA: right arm; LL: right leg; RL: right leg; LLRA: left leg with right arm; RLLA: right leg with left arm.

of time-frequency characteristics and distinguishability of channels are explained in parts D and E.

A. Participants and Experiment Protocol

Sixteen healthy and BCI-naïve human subjects (seven males, nine females; mean ± SD aged: 23.8 ± 1.9 years) were recruited in ME (seven subjects) and MI (nine subjects) experiments, respectively. They all had a normal or corrected-normal vision. Prior to the experiment, each of them gave their written informed consent and was confirmed to be right-handed according to the Edinburgh Handedness Inventory. The experiment protocol was carried out in accordance with the Declaration of Helsinki. The Human Participant Ethics Committee of the Southern University of Science and Technology approved this study (No. 20210024).

To make comparisons, four single-limb tasks and two compound-limbs tasks were designed in Fig. 1(a). Subjects were expected to execute or imagine the following actions: 1) the single upper limb swings forward and back (LA/RA); 2) the single leg kicks forward with the foot dorsiflexion and back to the original point (LL/RL); 3) the unilateral lower limb and the contralateral upper limb move simultaneously as described in single-limb action (LLRA/RLLA). The specific action process of one task was shown in Fig. 1 (b), taking the LLRA task as an example.

The processes of ME and MI experiments designed in this research were shown in Fig. 1 (c) and Fig. 1 (d). The whole ME and MI experiments were divided into eight and six sessions, respectively, and each section consisted of 36 trials. During each session, six tasks were randomly displayed. Between the two sessions, there would be an intermediate two-minute rest. Each trial included three stages: baseline, ME or MI, and rest. The total duration of each experiment was about 120 minutes, which included the device setting and instruction time for subjects. In each experiment, there was a video shown on the screen. In ME, subjects were required to perform actions shown in the video synchronously. In MI, subjects were instructed to familiarize themselves with the corresponding actual movements of imagery tasks for about 15 min. Then, at the formal MI experiment, the participants watched the video at first; after 2 s of baseline time, there would be a static picture of the task and then subjects started to imagine the specific action for about 4 s. In both ME and MI tasks, participants executed or imagined movement only once in a single trial. Table I summarized the important protocol parameters in ME and MI.

TABLE I
THE EXPERIMENTAL PROTOCOL PARAMETERS IN ME AND MI

	ME	MI
participants	7	9
recorded data type	56 EEG channels, 4 EOG channels, 4 EMG channels	56 EEG channels, 4 EOG channels
sampling frequency	1200Hz	1200Hz
re-sampling frequency	512Hz	512Hz
time of one trial	9s	13s
trials of one task	48	36

B. Data Acquisition and Preprocessing

The experiment was conducted in an electromagnetic-shielded environment, as shown in Fig. 2(a). Subjects sat on a chair located approximately 1.5m away from a 43-inch display monitor. They needed to lean against the chair with their backs straight, keeping their arms naturally vertical at two sides and

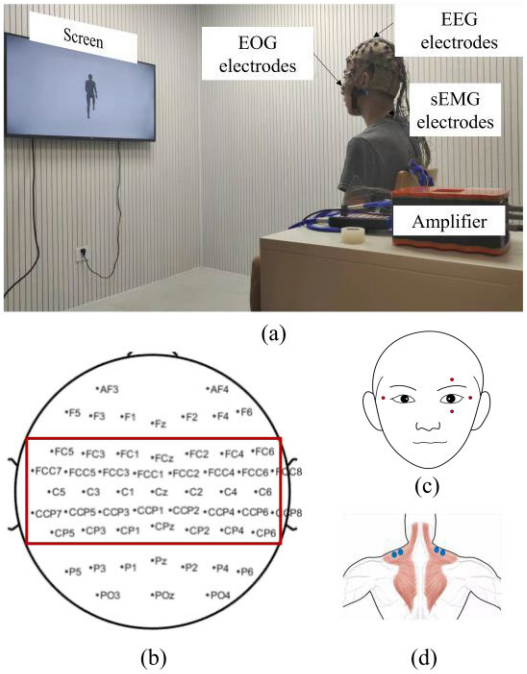

Fig. 2. The actual experimental environment (a), electrodes setup of EEG (b), EOG (c) and sEMG (d). Given the information of motor planning and control, electrodes in the red rectangle area were used for decoding.

their legs relaxed. This sitting state could avoid significant artifacts caused by limb movement in ME and the fatigue that might be caused by the long-time standing posture in both ME and MI. A 56-electrode EEG head cap shown in Fig. 2(b) was used and the locations of electrodes were set according to the 10-20 international placement system [32]. The referenced electrodes were placed on the earlobes, and the grounding electrode was placed on the forehead. EEG data were recorded by the 256-channel g.HIAMP biosignal amplifier (g.tec medical engineering GmbH, Austria) in a frequency range from 0.1Hz to 100Hz with a 1200Hz sampling frequency. Electrode impedances were kept to less than 30KΩ.

Besides, four electrooculography (EOG) electrodes were used in both ME and MI experiments. Two of them were placed above and below the left eye, and the other two were put on the outer canthus of eyes, which was shown in Fig. 2(c). The left EOG channel was referenced with the right EOG channel to represent the horizontal EOG component. Similarly, the upper one was referenced with the lower channels to capture the vertical EOG component. In addition, there were four surface-electromyography (sEMG) channels set at trapezius near the neck in pairs respectively (Fig. 2(d)) in ME experiments. The sEMG channels were referenced with their same-side channels, capturing the muscle electrical activities.

All data preprocessing was conducted via the EEGLAB toolbox [33] in MATLAB 2020a (The MathWorks, Natick MA). The EOG and EMG signals were filtered from 0.1Hz to 20Hz and 5Hz to 120Hz, respectively. The abnormal EEG channels were detected visually and interpolated. Then, the EEG signals were band-pass filtered from 1Hz to 30Hz. Next, we used the ASR function for correcting signals with artifacts. Subsequently, the EEG signals were re-referenced by the common average reference method [34]. Then, the independent component analysis (ICA) was applied and the artifactual component was deleted by making a comparison with the processed EOG and sEMG signals. After that, we also used the ICALABEL function [35] to remove the other residual artifacts. Finally, the EEG data were down-sampled to 512Hz.

C. Time-Frequency Analysis

Event-related spectral perturbation (ERSP) presents mean spectral power variations during the execution time compared with baseline time (pre-task). It described the even-related (de)synchronization (ERD/ERS) features of brain signals in time-frequency domain. To calculate the ERSP, the power spectrum is computed over a sliding window and then averaged across all trials, which can be defined as follows [36]:

$$ERSP(k, f, t) = \frac{(F_k(f,t))^2 - B(k,f)}{\sqrt{\frac{1}{T}\sum_t ((F_k(k,f,t))^2 - B(k,f))^2}} \quad (1)$$

where $F_k(k, f, t)$ is the spectral estimation of the channel k at frequency f f and time t, T denotes the number of discrete time points and t denotes the time point index. The B(k, f) $B(k, f)$ is the mean values of baseline interval, defined as follows:

$$B(k, f) = \frac{1}{T}\sum_t (F_k(k, f, t))^2 \quad (2)$$

In this research, the ERSP values were calculated from the 0.5 s before cue onset to 4.5 s after cue onset between 1 Hz and 30 Hz. The data form 0.5 s before cue onset to cue onset was determined as baseline data of each trial. Since the ERD/ERS phenomenon induced by one subject was not apparent, this study superimposed and averaged the time-frequency spectra of the evoked signals under all trials of all subjects in same tasks.

Topographic maps represent the mean ERSP values of all electrodes in the specific frequency band and time interval of EEG signals. In this research, we averaged ERSP values across all subjects to obtain a group-level ERSP topographic map that helped analyze the spatial scalp distribution of ERD/ERS information among the limb-related motor cortex.

D. Distinguishability of Motor-Related Channels

The EEG signals of different tasks correspond to different types of classes. Suppose the ERD amplitude of one task at all EEG channels in the specific frequency band is different from that of the other task at some electrodes. Then the two tasks can be distinguished. The Fisher score was used as the criterion of distinguishability in this paper. It is defined as [37]:

$$Fisher_{score} = \frac{|ERD_1 - ERD_2|^2}{\sigma_1^2 + \sigma_2^2} \quad (3)$$

$$ERD_k = \frac{P_{task} - P_{baseline}}{p_{baseline}} * 100 \quad (4)$$

$$P = \frac{1}{T}\int_{t_1}^{t_2} \left| fft(X_c^t) \right|^2 dt (T = t_2 - t_1) \quad (5)$$

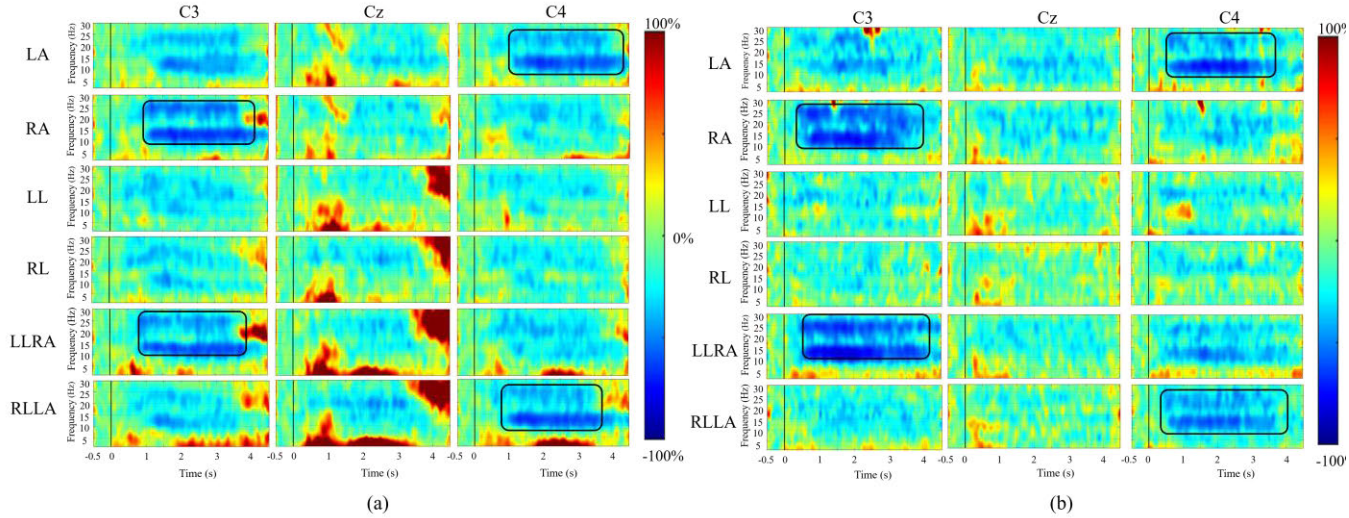

Fig. 3. Average ERSP figures of six tasks across all subjects at key electrodes C3, Cz, and C4 during ME (a) and MI (b) conditions. Red and blue indicates ERS and ERD respectively. The different time-frequency areas were marked with black borders. LA: left arm; RA: right arm; LL: right leg; RL: right leg; LLRA: left leg with right arm; RLLA: right leg with left arm.

where ERD_i (i=1, 2) represented the ERD of one task; σ_i represented the corresponding standard deviation of ERD;P represents the mean power spectrum density (PSD) of channel C. The Fisher score for each subject in each binary classification task was calculated on the 1 Hz-wide band. This band was named as subject-specific band due to it has the best classification performance obtained through SSCSP feature extraction method and machine learning algorithm. In this study, the threshold Fisher score level for each subject was set as the third quartile of Fisher scores across all tasks. The greater the Fisher score corresponding to a channel, the separability of the two tasks was greater.

E. Feature Extraction and Classification Methods

The Common Spatial Pattern (CSP) algorithm has been widely applied for EEG signal feature extraction. This method designs a spatial filter related to a specific task to maximize the variance of the one-class signal while minimizing the variance of the other-class signals. The K components related to a specific task were extracted, eliminating irrelevant components and noise [38]. Filter bank CSP (FBCSP) [39] is a is a variation of CSP. The full frequency bands were divided into multiple sub-bands; then the features of each band were extracted by the CSP filter; finally, the optimal K features among all sub-bands are selected by the feature selection algorithm.

In this study, the traditional CSP method was applied to data that was filtered from 4Hz to 30 Hz, which was the first feature extraction method. The second CSP method was named subject-specific CSP (SSCSP). The EEG data were filtered by a 1Hz interval from 1Hz to 30Hz, resulting in 29 frequency-band datasets. Next, the CSP was used to extract features on each sub-frequency band. Features of each sub-band were then used for classification through machine learning algorithms. The sub-frequency band that showed the best classification accuracy was determined as the subject-specific frequency band. The third feature extraction method is FBCSP. The EEG data were filtered by six filter banks, which were composed of 4-8 Hz, 8-12 Hz, 12-16 Hz, 16-20 Hz, 20-24 Hz, and 24-28 Hz. Then the best four features were selected from the 4*6=24 features by the Mutual Information-Based Best Individual Feature (MIBIF) algorithms. According to the ERSP analysis, preprocessed EEG data were extracted from 1 s to 4 s after the cue onset for feature extraction and classification.

Then, to avoid potential biases that may be introduced by using only one classifier, three classic machine learning algorithms were applied to classify the features of each paradigm. These algorithms included support vector machine (SVM), K-nearest neighbor (KNN), and random forest (RF). The classification tasks in each paradigm are as follows: (1) single-upper-limb tasks: LA and RA; (2) single-lower-limb tasks: LL and RL; (3) compound-limbs tasks: LLRA and. RLLA. The 10-fold stratified cross-validation was applied to evaluate the classification performance that presented by the average accuracy.

III. Results

To investigate the feasibility of the proposed paradigm, this section first analyzes the results of time-frequency domain features in each type of task and then presents the final classification results. In Parts A, B, and C, the characteristics of the event-related spectral perturbation, the brain spatial activation distribution, and the separability of motor-related channels are described, respectively. Finally, the classification results are shown in part D.

A. Event-Related Spectral Perturbation

The event-related spectral perturbation across 1Hz to 30Hz at electrodes C3, C4 and Cz of all subjects were shown in Fig. 3. Noticeably, for all action patterns, long-lasting power decreases around 1s at C3, Cz, and C4 electrodes after cue onset, in both MI and ME. In the single-upper-limb swing

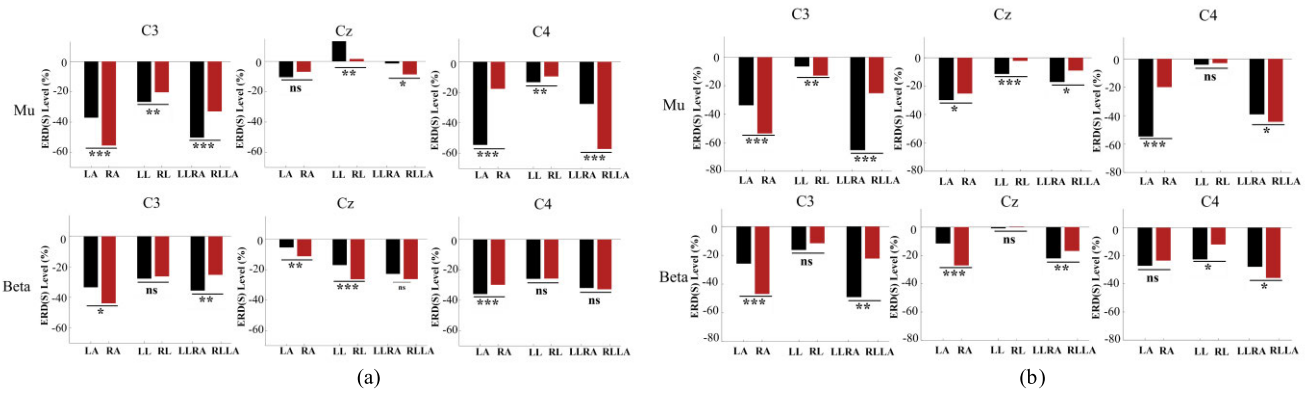

Fig. 4. The ERD amplitude at C3, Cz and C4 electrodes in (a) ME and (b) MI conditions. *, **, *** represented that the p-value of one-way ANOVA test is lower than 0.05, 0.01 and 0.001 respectively.

task (LA and RA), for example, when subjects executed or imagined the action of the left upper limb, stronger ERD was shown at C4 than at C3. In contrast, no obvious difference between tasks of the single left leg and right leg (LL and RL) could be found. However, while combining actions of both arm and leg, it was easy to differentiate LLRA and RLLA tasks by contrasting the ERD responses at C3 and C4. Specifically, for the LLRA task, there was more lasting and distinct ERD at electrode C3. Its feature bands included 10-15Hz and 20-28Hz, which covered the mu and beta rhythms. For the RLLA task, the feature bands were similar to the LLRA task, but its feature electrode was C4. In terms of Cz, there showed stronger ERD around 20Hz in RL, LLRA and RLLA tasks during the ME condition; while in the MI state, the stronger ERD phenomenon only showed in single-upper-limb tasks.

The grand average amplitude of ERD(S) at mu and beta frequency bands were presented in Fig. 4. It could be seen that at the mu band, the difference between (1) LA and RA or (2) LLRA and RLLA at C3 and C4 were significant. For the electrode Cz, the significance level between LL and RL was higher than the other two types of tasks in ME. However, there was no significant difference between LL and RL tasks at the beta band in MI.

B. Brain Spatial Activation Distribution

From Fig. 5, it was found that the ERD phenomenon is more obvious in the mu and higher beta frequency bands. Therefore, the following contents will discuss and analyze the ERD topography in these two frequency bands. The one-dimensional characteristic data of ERD was obtained by averaging the time-frequency data in frequency and time windows. In Fig. 5, the brain topographies of six tasks were averaged across all subjects for ME and MI, respectively.

In both MI and ME conditions, there was a larger ERD area in the motor cortex at mu rhythm. To be specific, for the single-upper-limb task, the brain topographic map of the left upper limb showed that the attenuation of EEG power at the right brain region was more obvious than that of the left region. A similar contralateral dominance phenomenon also showed in the right upper-limb task. For single-lower-limb tasks, the difference between LL and RL was not distinct as that of single-upper-limb tasks. The common characteristic was that broader ERD showed at the central area both in LL and RL tasks. Nevertheless, compared with the single-lower-limb task, the substantial ERD phenomenon of compound limbs showed both at the contralateral hemisphere and the central SMA area, which reflected the activities of both the unilateral lower limb and the contralateral upper limb. However, as for the beta rhythm, the distinct contralateral dominant phenomenon only appeared in the compound-limbs tasks.

Furthermore, we compared the difference in induced ERD between MI and ME. Overall, the ERD feature difference was consistent in MI and ME. However, there still had some distinctions. For example, the noticeable ERD was also shown at the frontal and occipital lobes on the LA task. For the single-leg task, the ERD of LL was intense around electrode C2. For the compound-limbs task, unlike the ME condition, the ERD in the beta band presents contralateral distribution in compound-limbs MI tasks.

C. Separability Analysis of Motor-Related Channels

Fig. 6 and Fig. 7 showed the Fisher analysis of motor-related channels in three two-class classification tasks for all subjects in two situations. The top sub-figures in each figure presented the Fisher scores of each EEG electrode. The blue dotted lines were the subject-specific threshold levels. From Fig 6 (a) and Fig 7 (a), it could be seen that the number of channels that exceeded the threshold level in single-upper-limb paradigm and compound-limbs paradigm was larger than that of single-lower-limb paradigm for most of the subjects.

Fig. 6 (b) and Fig. 7 (b) showed the distribution of channels (red) that exceeded the threshold level. In single-upper-limb paradigm, the highly separable channels usually appeared at/around C3 and C4. For single-lower-limb paradigm, it showed that most of the red channels neared channel Cz. In terms of compound-limbs paradigm, the highly separable channels showed not only on the upper-limb controlled area but also around Cz. In addition, more than half of the subjects had overlapping red channels between single-upper-limb and compound-limbs paradigms.

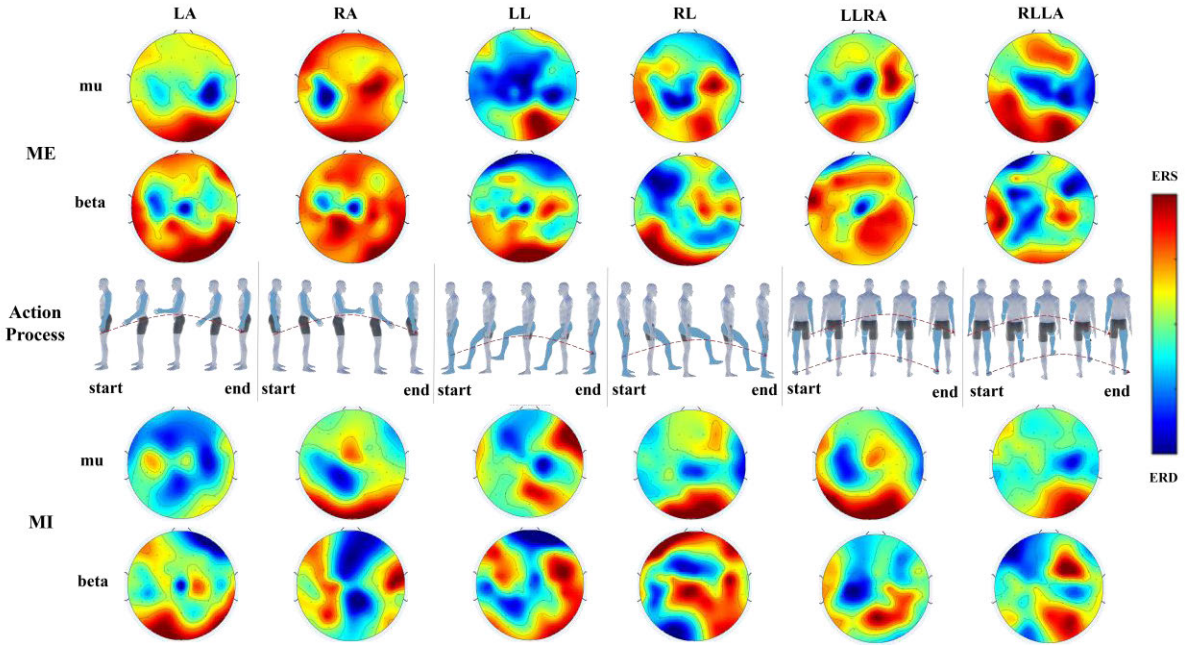

Fig. 5. The average brain topographical distribution based on ERSP values for the motor execution and motor imagery conditions respectively.

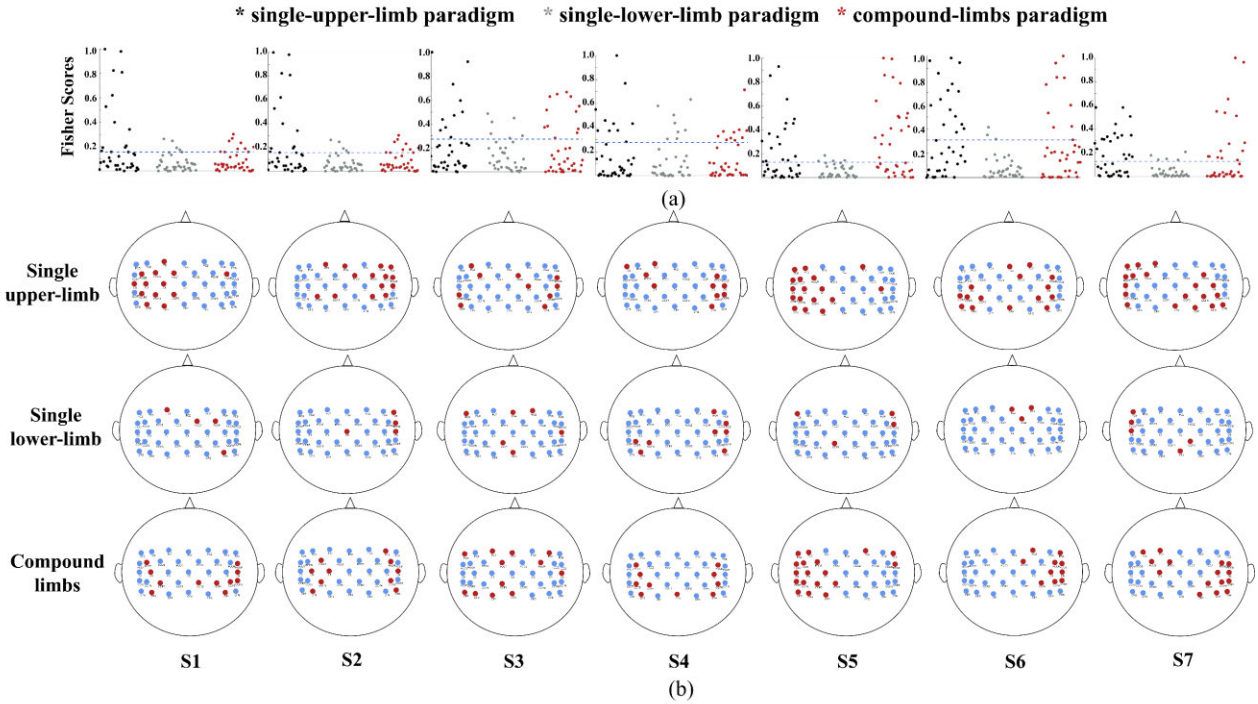

Fig. 6. Fisher scores of electrodes covering motor cortex in ME condition. The spatial maps showed the EEG electrodes that exceeded the threshold level (red) in different tasks and conditions. The blue dotted lines represented threshold levels.

D. Classification Performance

The performance of all subjects who participated in ME and MI experiments was illustrated in Table II and Table III, respectively. First of all, it is apparent that there was the same classification performance phenomenon in both ME and MI: single-upper-limb task > compound-limbs task > single-lower-limb task. Besides, for all three paradigms in ME and MI, the average accuracies of the SSCSP method were always the highest, followed by the FBCSP, and the CSP is the worst.

Take the results of the SSCSP as examples, mean accuracy of compound-limbs tasks was as well as that of single-upper-limb tasks in ME, with about 2% difference. Five of seven subjects' accuracies were higher than 90% in compound-limbs tasks. In contrast, the best average accuracy of single-lower-limb tasks was 64.91% ± 6.67%. In MI, accuracies of

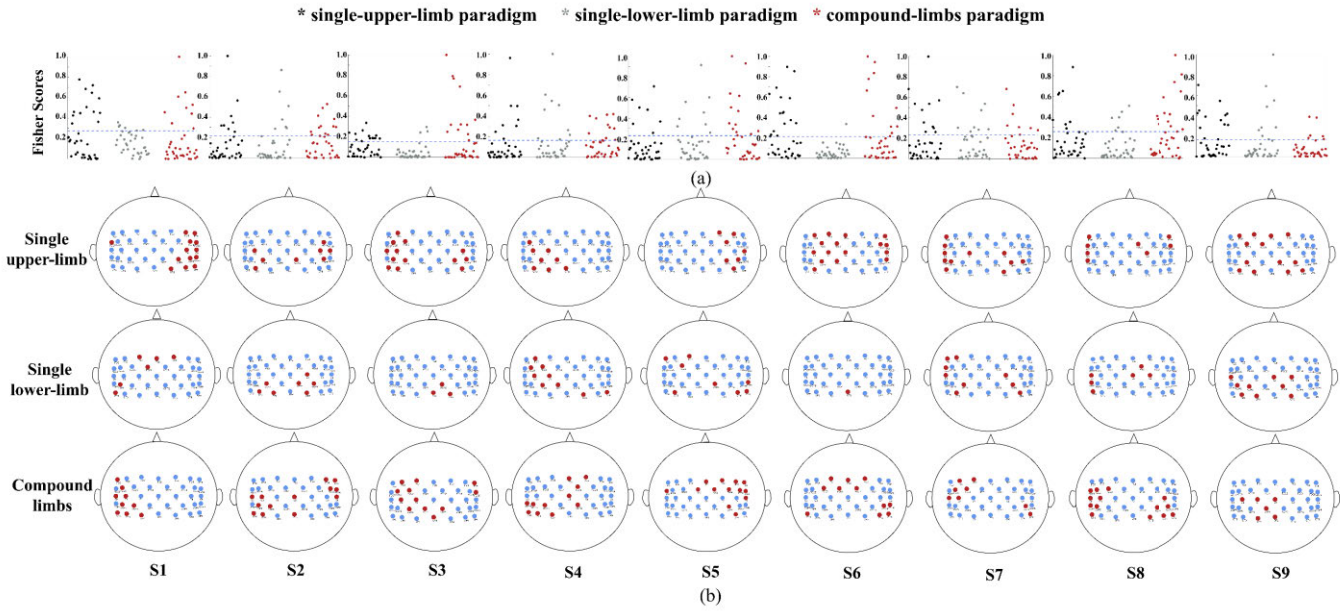

Fig. 7. Fisher scores of electrodes covering motor cortex in MI condition. The spatial maps showed the EEG electrodes that exceeded the threshold level (red) in different tasks and conditions. The blue dotted lines represented threshold levels.

TABLE II
AVERAGE ACCURACY IN MOTOR EXECUTION (%)

Subject		Single-upper- limb paradigm			Single-lower-limb paradigm			Compound-limbs paradigm		
		CSP	SSCSP	FBCSP	CSP	SSCSP	FBCSP	CSP	SSCSP	FBCSP
S1	SVM	93.81	96.90	96.67	58.81	68.81	32.62	75.00	94.33	**96.67**
	KNN	94.29	96.90	96.67	**60.48**	65.95	41.43	**77.00**	93.00	94.67
	RF	95.24	98.33	95.00	59.05	70.24	43.10	75.00	96.33	93.33
S2	SVM	84.82	97.32	90.36	41.25	54.64	45.00	66.07	91.07	89.46
	KNN	74.11	**98.75**	90.36	44.11	58.39	46.25	59.82	89.82	88.21
	RF	82.50	98.75	94.46	46.25	60.54	46.61	61.07	92.5	90.71
S3	SVM	63.33	75.56	75.56	57.22	72.22	57.36	57.50	80.97	64.58
	KNN	68.89	68.89	76.67	66.67	71.53	**61.94**	54.03	79.86	66.81
	RF	70.00	77.78	66.67	60.00	**73.61**	57.36	52.78	78.61	64.72
S4	SVM	54.29	72.86	71.43	44.52	67.86	45.48	51.67	61.67	50.00
	KNN	48.57	75.71	61.43	50.48	60.24	47.38	43.33	65.00	53.33
	RF	48.57	74.29	62.86	53.57	61.19	47.38	50.00	66.67	41.67
S5	SVM	72.14	97.32	80.36	43.81	61.32	39.29	75.71	94.29	78.57
	KNN	72.32	96.07	81.61	53.57	65.71	44.05	84.29	94.29	84.29
	RF	73.75	94.64	81.61	53.81	63.10	42.38	81.43	95.71	81.43
S6	SVM	91.67	95	96.67	44.52	65	42.86	93.00	94.33	92.67
	KNN	93.33	95	93.33	44.52	62.85	41.19	93.33	94.33	87.67
	RF	93.33	95	98.33	42.62	60.24	45.95	91.33	95	91.00
S7	SVM	95.71	98.57	92.86	31.90	58.81	55.71	91.67	**100.00**	94.67
	KNN	91.43	98.57	95.71	34.76	68.33	54.29	91.67	98.57	94.67
	RF	**97.14**	98.57	**98.57**	36.90	63.33	54.05	96.33	98.33	96.33
MEAN ±SD	SVM	79.40 ± 16.31	90.50 ± 11.21	**86.27 ± 10.38**	46.01 ± 9.31	64.09 ± 6.17	45.47 ± 8.73	**72.95 ± 15.83**	88.09 ± 13.01	80.95 ± 17.68
	KNN	77.56 ± 16.71	88.99 ± 12.31	85.11 ± 12.82	**50.65 ± 10.76**	**64.72 ± 4.57**	48.08 ± 7.73	71.92 ±19.63	88.04 ± 11.88	**81.38 ± 15.53**
	RF	**80.08 ± 17.50**	**91.05 ± 10.45**	85.36 ± 15.21	50.31 ± 8.65	64.61 ± 5.23	**48.12 ± 5.57**	72.56 ± 18.41	**89.02 ± 12.84**	79.89 ± 19.94

all tasks had declined. The highest average accuracies of single-upper-limb paradigm, single-lower-limb paradigm, and compound-limbs paradigm declined to 79.38%, 62.98% and 73.70%, respectively. However, there were still three subjects whose classification performance of compound-limbs tasks was between 80% and 90%.

One-way ANOVA statistical analysis was performed to further compare the classification performance differences between compound-limbs paradigm and single-limb paradigms across combinations of three feature extraction methods and three classification algorithms, which was shown in Fig. 8. It could be found that there was no significant

TABLE III
AVERAGE ACCURACY IN MOTOR IMAGERY (%)

Subject		Single-upper- limb paradigm			Single-lower-limb paradigm			Compound-limbs paradigm		
		CSP	SSCSP	FBCSP	CSP	SSCSP	FBCSP	CSP	SSCSP	FBCSP
S1	SVM	53.93	**93.04**	62.32	37.86	61.79	36.79	73.57	**90.00**	62.86
	KNN	51.43	91.61	66.43	35.00	61.96	45.18	71.96	88.75	69.64
	RF	54.11	84.82	63.57	33.75	65.00	33.93	69.29	86.07	65.54
S2	SVM	63.33	81.67	**77.86**	41.67	58.33	46.67	57.86	85.24	55.95
	KNN	58.57	82.14	75.24	43.33	58.33	51.67	52.62	81.90	57.86
	RF	60.00	78.10	70.71	38.33	61.96	41.67	59.05	80.71	54.29
S3	SVM	**74.82**	90.36	73.57	39.29	69.46	**52.86**	72.50	92.86	79.11
	KNN	70.36	93.04	68.75	45.00	64.11	51.79	75.36	89.11	**79.29**
	RF	71.79	84.82	66.25	43.57	66.79	54.11	**79.29**	89.11	77.68
S4	SVM	73.57	84.64	73.93	50.18	**70.89**	47.50	62.86	67.32	60.00
	KNN	68.04	76.43	72.32	45.89	66.43	40.89	54.29	79.46	59.82
	RF	72.14	77.68	72.68	51.25	65.18	48.75	57.14	65.36	60.00
S5	SVM	48.93	85.00	43.39	27.86	58.93	37.68	38.21	70.71	47.86
	KNN	44.82	85.18	47.50	37.50	57.50	37.50	40.36	76.43	51.96
	RF	38.93	90.71	48.75	29.29	57.86	32.14	35.18	77.68	57.68
S6	SVM	51.00	68.67	68.67	50.33	62.00	44.00	43.67	62.33	52.33
	KNN	43.33	65.00	68.67	39.33	64.33	38.67	47.00	62.67	56.00
	RF	51.33	73.00	62.67	44.67	58.67	38.33	47.00	61.00	57.33
S7	SVM	50.89	65.18	57.68	42.68	61.43	47.68	51.43	64.29	40.00
	KNN	51.07	69.11	57.86	45.36	65.71	49.46	55.71	65.71	41.43
	RF	46.79	65.71	59.29	41.61	61.61	46.25	54.29	60.00	47.14
S8	SVM	55.71	76.07	43.21	44.64	58.75	54.29	44.82	62.50	52.14
	KNN	54.29	74.64	43.39	51.25	55.18	55.54	43.04	66.43	52.32
	RF	50.36	70.36	43.39	45.89	62.86	55.54	37.68	59.82	52.32
S9	SVM	74.11	69.82	74.11	51.25	62.50	37.68	35.89	55.89	35.71
	KNN	76.43	71.43	69.82	48.04	61.07	37.68	41.79	52.86	38.75
	RF	67.14	66.96	74.11	**59.46**	62.50	41.79	37.32	61.07	34.46
MEAN ±SD	SVM	**60.70 ±10.90**	**79.38 ±9.94**	**63.86 ± 13.25**	42.86 ±7.48	**62.68 ±4.54**	45.01 ± 6.52	53.42 ±14.10	72.35 ±13.51	54.00 ± 12.86
	KNN	57.59 ±11.65	78.73 ±9.88	63.33 ± 11.24	**43.41 ±5.22**	61.63 ±3.92	**45.37 ± 6.96**	**53.57 ±12.68**	**73.70 ±12.47**	**56.34 ± 12.67**
	RF	56.95 ±11.59	76.91 ±8.66	62.38 ± 10.52	43.09 ±9.00	62.49 ±2.94	43.61 ± 8.26	52.91 ±15.19	71.20 ±12.09	56.27 ± 11.93

difference between compound-limbs tasks and single-upper-limb tasks in both ME and MI. As for comparison with single-lower-limb paradigm, the classification performance of compound-limbs paradigm was significantly ($p < 0.05$) better than that of single-lower-limb tasks across all methods in ME. But in MI, its performance was only significant in (1) combinations of KNN and three feature extraction methods, and (2) combination of RF and FBCSP methods.

IV. DISCUSSION

This study proposed a compound-limbs EEG-BCI paradigm that integrated upper-limb swing and lower-limb stepping. This paradigm not only activated more brain regions but also had better classification performance. The feasibility and effectiveness of the proposed paradigm were verified in four aspects: (1) the event-related spectral perturbation characteristics, (2) the brain spatial activation distribution, (3) the separability of EEG electrodes, and (4) the classification performance. These results are discussed in detail as follows.

From the ERSP result, the contralateral dominance effect was not found in the single-lower-limb tasks. The ERD amplitude results of LL and RL tasks suggested that more neural activities were induced at C3 and C4 than that at Cz, which was further verified in the ERSP topographical distribution. As for the single-upper-limb tasks, the significant contralateral dominance characteristic was consistent with the previous studies [40], [41]. In terms of the focus paradigm of this study, as we expected, when combing the unilateral lower limb with the contralateral upper limb, the brain activation level was increased compared with the single-lower-limb tasks. The possible explanation was that the participation of upper limb swing action made a contribution to the ERD increase, which was also found in [30]. In addition, the ERSP topographical distribution maps (Fig. 4) among all tasks verified that compound-limbs tasks activated not only the contralateral hemisphere areas that were related to upper-limb actions but also activated the central parietal region that controls lower limbs, which was a similar phenomenon in [26]. However, according to ERSP analysis of the single limb task, contralateral lower limb movements may also activate the ipsilateral upper limb control area. Therefore, it could be noted that there was an overlap of activated electrode areas between the LLRA and RLLA tasks.

The separability analysis of motor-related channels from all subjects revealed that the number of distinguishable channels of compound-limbs tasks was much more than that of

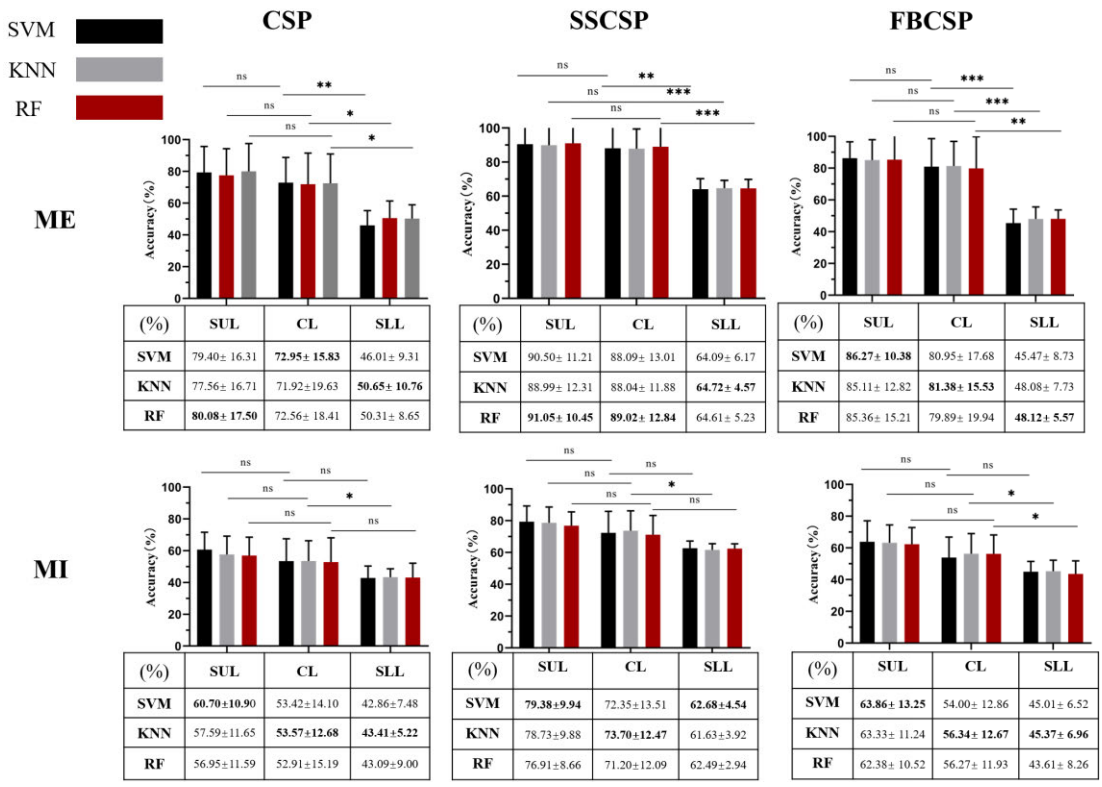

ME (%)	SUL	CL	SLL
SVM	79.40± 16.31	**72.95± 15.83**	46.01± 9.31
KNN	77.56± 16.71	71.92±19.63	**50.65± 10.76**
RF	**80.08± 17.50**	72.56± 18.41	50.31± 8.65

ME (%)	SUL	CL	SLL
SVM	90.50± 11.21	88.09± 13.01	64.09± 6.17
KNN	88.99± 12.31	88.04± 11.88	**64.72± 4.57**
RF	**91.05± 10.45**	**89.02± 12.84**	64.61± 5.23

ME (%)	SUL	CL	SLL
SVM	**86.27± 10.38**	80.95± 17.68	45.47± 8.73
KNN	85.11± 12.82	**81.38± 15.53**	48.08± 7.73
RF	85.36± 15.21	79.89± 19.94	**48.12± 5.57**

MI (%)	SUL	CL	SLL
SVM	**60.70±10.90**	53.42±14.10	42.86±7.48
KNN	57.59±11.65	**53.57±12.68**	**43.41±5.22**
RF	56.95±11.59	52.91±15.19	43.09±9.00

MI (%)	SUL	CL	SLL
SVM	**79.38±9.94**	72.35±13.51	**62.68±4.54**
KNN	78.73±9.88	**73.70±12.47**	61.63±3.92
RF	76.91±8.66	71.20±12.09	62.49±2.94

MI (%)	SUL	CL	SLL
SVM	**63.86± 13.25**	54.00± 12.86	45.01± 6.52
KNN	63.33± 11.24	**56.34± 12.67**	**45.37± 6.96**
RF	62.38± 10.52	56.27± 11.93	43.61± 8.26

Fig. 8. The classification performance and one-way ANOVA test of three classifiers combined with three feature extraction methods on two experimental conditions. CL: compound-limbs paradigm; SUL: single-upper-limb paradigm; SLL: single-lower-limb paradigm.*, **, ** indicated that the $p < 0.05$, $p < 0.01$, $p < 0.001$, respectively.

single-lower-limb tasks in ME and MI, explaining the higher classification results of compound-limbs tasks. A comparison of this result with those of [25] confirmed that the regions related to the left and right lower limbs were overlapping and challenging to differentiate based on EEG signals. Besides, for single-upper-limb and compound-limb paradigms, most of electrodes that passed the threshold were the lateral ones. It is consistent with the brain spatial ERSP distribution result that the ERD phenomenon was distinct on the lateral side of motor cortex area.

Three feature extraction methods and three machine learning algorithms were adopted in this study. It is consistent with the suggestion of previous studies that the performance of the FBCSP method was better than that of traditional CSP method. However, there is a new finding in this study that using the SSCSP method improved the classification performance. Especially in the MI condition, the accuracies of SSCSP were about 16% higher than those of FBCSP. This suggested that extracting features from subject-specific 1Hz-width frequency bands might provide more effective and task-related information. Therefore, the matching of the subject-specific frequency band and paradigms probably should be considered.

In terms of the performance of the proposed compound-limbs paradigm, the proposed compound-limbs EEG-BCI paradigm realized a higher classification accuracy of human stepping patterns than that of the single-lower-limb EEG-BCI paradigm. Based on the result of the SSCSP method, the best average accuracies of the compound-limbs paradigm under two conditions were 24.30% (ME) and 11.02% (MI) higher than those of the single-lower-limb paradigm. Besides, the average performance of the compound-limbs MI paradigm was 2.45%, 7.2%, and 13.95% higher than that of the previous single-leg paradigms [21], [23], [24], respectively. In Fig. 8, although the classification performance of the compound-limbs paradigm was not always significantly better than that of the single-lower-limb paradigm in MI, it could be verified that the involvement of upper-limb action is advantageous for classifying the patterns of human stepping based on statistical significance test results of ME. In fact, some people might not have the adequate ability to execute the MI task. These people are defined as BCI illiteracy [42]. Although the multi-limb task could activate more motor cortex [43], [44], it also depends on more concentration. Therefore, subjects with lower accuracies of compound-limbs MI tasks may have a poor ability to imagine multi-limbs movement at the same time. These subjects might need more practice for the adaptation of these imagination tasks. Besides, it should also be noted that the highest average accuracies of the compound-limbs paradigm were 2.03% (ME) and 5.68% (MI) lower than those of the single-upper-limb paradigm. The overlapping activation regions between the LLRA and RLLA tasks may affect the degree of difference in features, making it more difficult to distinguish between them than the single-upper-limb tasks. Some studies found that the ipsilateral cortex was also activated during

the single upper-limb movement [45]. There existed similar neural signal activities between ipsilateral and contralateral hemispheres [46]. Besides, it was reported that the lower-limb movement showed less lateralization in the motor cortex [47]. Based on these single upper-limb findings, we proposed a hypothesis that compound-limbs tasks might produce more similar neural activities in both upper-limb and lower-limb motor control cortex areas. Therefore, the classification accuracy of compound-limbs tasks could be lower than that of the single-upper-limb tasks. However, benefiting from larger activation levels of upper limbs, the difference between compound-limbs tasks was easier to be decoded than that of single-lower-limb tasks.

Although the classification accuracy of the single-upper-limb paradigm was better than the proposed paradigm, the single-upper-limb paradigm is not a natural and direct way to reflect human walking intention. In terms of the previous hand-foot paradigm [26], [27], [28], the imagination of playing drums is still not similar with compound-limbs action of human walking. In contrast, the proposed paradigm involved simultaneous actions of the unilateral lower limb and the contralateral upper limb, which is closer to the natural human stepping posture. Besides, it is suggested that the swing of the upper limbs plays an important role in human walking [30], [48]. One of the advantages of this proposed compound-limbs paradigm is that it might be beneficial for gait rehabilitation, such as improving interlimb coordination and trunk stability after stroke [49], [50]. Therefore, the possible application of the proposed compound-limbs paradigm is to drive lower-limb rehabilitation exoskeletons by decoding human MI information. This system might not only present superior performance in decoding human stepping intentions but also contribute to coordination ability improvement between upper and lower limbs.

Despite the fact that this work proposed and proved the feasibility of the new paradigm for recognizing human walking intention based on EEG signals, there are several limitations worthing mentioned for practical applications. First, developing a fast and effective EEG online preprocessing platform is challenging. Signal quality plays an important role in online classification performance. Therefore, we have to exploit a real-time artifact-reduction algorithm to improve the signal quality. Second, considering BCI systems requiring robust decoding abilities in real-time scenarios [51], [52], the current offline decoding accuracy (73.70%) needs to be further improved in terms of feature extraction and decoding models. Third, the current compound-limbs ME paradigm may not be appropriate for patients since they generally have difficulty in moving their upper and lower limbs coordinatively and naturally.

V. Conclusion

This study proposed a new compound-limbs BCI paradigm to decode the human lower-limb stepping intention from EEG. The paradigm involved both the stepping action of the unilateral lower limb and the swing action of the contralateral upper limb simultaneously. With the analysis of EEG characteristics, it can be seen that compound-limbs tasks activated both upper- and lower-limb-related brain regions and generated an evident difference between the stepping intention of the left and right sides. Furthermore, the average classification accuracies of compound-limbs paradigm were higher than those of the single-lower-limb paradigm on both the ME- and MI-EEG dataset. These findings demonstrated that decoding step intention from compound-limbs tasks is feasible and outperforms the traditional single-lower-limb paradigm. Future work will focus on integrating this EEG-BCI paradigm in real-life walking-assistive exoskeletons.

VI. Supplementary Materials

The experimental video is attached along with the paper.

References

[1] R. Abiri et al., "A comprehensive review of EEG-based brain-computer interface paradigms," *J. Neural Eng.*, vol. 16, no. 1, Feb. 2019, Art. no. 011001.

[2] P. Arpaia, A. Esposito, A. Natalizio, and M. Parvis, "How to successfully classify EEG in motor imagery BCI: A metrological analysis of the state of the art," *J. Neural Eng.*, vol. 19, no. 3, Jun. 2022, Art. no. 031002.

[3] H. Yuan and B. He, "Brain–computer interfaces using sensorimotor rhythms: Current state and future perspectives," *IEEE Trans. Biomed. Eng.*, vol. 61, no. 5, pp. 1425–1435, May 2014.

[4] X. Zhang, L. Yao, X. Wang, J. Monaghan, D. McAlpine, and Y. Zhang, "A survey on deep learning-based non-invasive brain signals: Recent advances and new frontiers," *J. Neural Eng.*, vol. 18, no. 3, Jun. 2021, Art. no. 031002.

[5] K. K. Ang and C. Guan, "EEG-based strategies to detect motor imagery for control and rehabilitation," *IEEE Trans. Neural Syst. Rehabil. Eng.*, vol. 25, no. 4, pp. 392–401, Apr. 2017.

[6] K. J. Miller, G. Schalk, E. E. Fetz, M. den Nijs, J. G. Ojemann, and R. P. N. Rao, "Cortical activity during motor execution, motor imagery, and imagery-based online feedback," *Proc. Nat. Acad. Sci. USA*, vol. 107, no. 9, pp. 4430–4435, Mar. 2010.

[7] M. A. Lebedev and M. A. L. Nicolelis, "Brain-machine interfaces: From basic science to neuroprostheses and neurorehabilitation," *Physiolog. Rev.*, vol. 97, no. 2, pp. 767–837, Apr. 2017.

[8] Y. T. He et al., "Brain-machine interfaces for controlling lower-limb powered robotic systems," *J. Neural Eng.*, vol. 15, no. 2, p. 15, Apr. 2018.

[9] G. Vingerhoets, F. P. de Lange, P. Vandemaele, K. Deblaere, and E. Achten, "Motor imagery in mental rotation: An fMRI study," *NeuroImage*, vol. 17, no. 3, pp. 1623–1633, Nov. 2002.

[10] A. Schwarz, P. Ofner, J. Pereira, A. I. Sburlea, and G. R. Müller-Putz, "Decoding natural reach-and-grasp actions from human EEG," *J. Neural Eng.*, vol. 15, no. 1, Dec. 2017, Art. no. 016005.

[11] T. Pistohl, A. Schulze-Bonhage, A. Aertsen, C. Mehring, and T. Ball, "Decoding natural grasp types from human ECoG," *NeuroImage*, vol. 59, no. 1, pp. 248–260, Jan. 2012.

[12] L.-W. Ko et al., "Integrated gait triggered mixed reality and neurophysiological monitoring as a framework for next-generation ambulatory stroke rehabilitation," *IEEE Trans. Neural Syst. Rehabil. Eng.*, vol. 29, pp. 2435–2444, 2021.

[13] B. Lei et al., "Walking imagery evaluation in brain computer interfaces via a multi-view multi-level deep polynomial network," *IEEE Trans. Neural Syst. Rehabil. Eng.*, vol. 27, no. 3, pp. 497–506, Mar. 2019.

[14] L. Ferrero, M. Ortiz, V. Quiles, E. Iáñez, and J. M. Azorín, "Improving motor imagery of gait on a brain–computer interface by means of virtual reality: A case of study," *IEEE Access*, vol. 9, pp. 49121–49130, 2021.

[15] K. Lee, D. Liu, L. Perroud, R. Chavarriaga, and J. D. R. Millán, "A brain-controlled exoskeleton with cascaded event-related desynchronization classifiers," *Robot. Auto. Syst.*, vol. 90, pp. 15–23, Apr. 2017.

[16] H. Gao et al., "EEG-based volitional control of prosthetic legs for walking in different terrains," *IEEE Trans. Autom. Sci. Eng.*, vol. 18, no. 2, pp. 530–540, Apr. 2021.

[17] C. Wang, X. Wu, Z. Wang, and Y. Ma, "Implementation of a brain-computer interface on a lower-limb exoskeleton," *IEEE Access*, vol. 6, pp. 38524–38534, 2018.

[18] Y. Hashimoto and J. Ushiba, "EEG-based classification of imaginary left and right foot movements using beta rebound," *Clin. Neurophysiol.*, vol. 124, no. 11, pp. 2153–2160, Nov. 2013.

[19] M. Tariq, P. M. Trivailo, and M. Simic, "Mu-beta event-related (de)synchronization and EEG classification of left-right foot dorsiflexion kinaesthetic motor imagery for BCI," *PLoS ONE*, vol. 15, no. 3, Mar. 2020, Art. no. e0230184.

[20] L. Gu, Z. Yu, T. Ma, H. Wang, Z. Li, and H. Fan, "EEG-based classification of lower limb motor imagery with brain network analysis," *Neuroscience*, vol. 436, pp. 93–109, Jun. 2020.

[21] W.-C. Hsu, L.-F. Lin, C.-W. Chou, Y.-T. Hsiao, and Y.-H. Liu, "EEG classification of imaginary lower limb stepping movements based on fuzzy support vector machine with kernel-induced membership function," *Int. J. Fuzzy Syst.*, vol. 19, no. 2, pp. 566–579, Apr. 2017.

[22] Y.-H. Liu, L.-F. Lin, C.-W. Chou, Y. Chang, Y.-T. Hsiao, and W.-C. Hsu, "Analysis of electroencephalography event-related desynchronisation and synchronisation induced by lower-limb stepping motor imagery," *J. Med. Biol. Eng.*, vol. 39, no. 1, pp. 54–69, Feb. 2019.

[23] A. Kline, N. D. Forkert, B. Felfeliyan, D. Pittman, B. Goodyear, and J. Ronsky, "FMRI-informed EEG for brain mapping of imagined lower limb movement: Feasibility of a brain computer interface," *J. Neurosci. Methods*, vol. 363, Nov. 2021, Art. no. 109339.

[24] A. Kline, C. G. Ghiroaga, D. Pittman, B. Goodyear, and J. Ronsky, "EEG differentiates left and right imagined lower limb movement," *Gait Posture*, vol. 84, pp. 148–154, Feb. 2021.

[25] M. Wieser, J. Haefeli, L. Bütler, L. Jäncke, R. Riener, and S. Koeneke, "Temporal and spatial patterns of cortical activation during assisted lower limb movement," *Exp. Brain Res.*, vol. 203, no. 1, pp. 181–191, May 2010.

[26] W. Yi, S. Qiu, H. Qi, L. Zhang, B. Wan, and D. Ming, "EEG feature comparison and classification of simple and compound limb motor imagery," *J. NeuroEng. Rehabil.*, vol. 10, no. 1, p. 106, Oct. 2013.

[27] W. Yi et al., "Evaluation of EEG oscillatory patterns and cognitive process during simple and compound limb motor imagery," *PLoS ONE*, vol. 9, no. 12, Dec. 2014, Art. no. e114853.

[28] W. Yi et al., "EEG oscillatory patterns and classification of sequential compound limb motor imagery," *J. NeuroEng. Rehabil.*, vol. 13, no. 1, p. 11, Jan. 2016.

[29] J. B. Weersink, N. M. Maurits, and B. M. de Jong, "EEG time-frequency analysis provides arguments for arm swing support in human gait control," *Gait Posture*, vol. 70, pp. 71–78, May 2019.

[30] J. B. Weersink, N. M. Maurits, T. van Laar, and B. M. de Jong, "Enhanced arm swing improves parkinsonian gait with EEG power modulations resembling healthy gait," *Parkinsonism Rel. Disorders*, vol. 91, pp. 96–101, Oct. 2021.

[31] R. Ma, Y. Jiang, Y. Chen, and M. Zhang, "A new EEG-based paradigm for classifying intention of compound-limbs movement," in *Proc. IEEE Int. Conf. Real-time Comput. Robot. (RCAR)*, Jul. 2022, pp. 63–68.

[32] R. Oostenveld and P. Praamstra, "The five percent electrode system for high-resolution EEG and ERP measurements," *Clin. Neurophysiol.*, vol. 112, no. 4, pp. 713–719, Apr. 2001.

[33] A. Delorme and S. Makeig, "EEGLAB: An open source toolbox for analysis of single-trial EEG dynamics including independent component analysis," *J. Neurosci. Methods*, vol. 134, no. 1, pp. 9–21, Mar. 2004.

[34] D. J. McFarland, L. M. McCane, S. V. David, and J. R. Wolpaw, "Spatial filter selection for EEG-based communication," *Electroencephalogr. Clin. Neurophysiol.*, vol. 103, no. 3, pp. 386–394, Sep. 1997.

[35] L. Pion-Tonachini, K. Kreutz-Delgado, and S. Makeig, "ICLabel: An automated electroencephalographic independent component classifier, dataset, and website," *NeuroImage*, vol. 198, pp. 181–197, Sep. 2019.

[36] J. Müller-Gerking, G. Pfurtscheller, and H. Flyvbjerg, "Designing optimal spatial filters for single-trial EEG classification in a movement task," *Clin. Neurophysiol.*, vol. 110, no. 5, pp. 787–798, May 1999.

[37] K. Keng Ang, Z. Yang Chin, H. Zhang, and C. Guan, "Filter bank common spatial pattern (FBCSP) in brain-computer interface," in *Proc. IEEE Int. Joint Conf. Neural Netw. (IEEE World Congr. Comput. Intell.)*, Jun. 2008, pp. 2390–2397.

[38] Y.-C. Jiang et al., "Characterization of bimanual cyclical tasks from single-trial EEG-fNIRS measurements," *IEEE Trans. Neural Syst. Rehabil. Eng.*, vol. 30, pp. 146–156, 2022.

[39] M. Gan and L. Zhang, "Iteratively local Fisher score for feature selection," *Int. J. Speech Technol.*, vol. 51, no. 8, pp. 6167–6181, Aug. 2021.

[40] G. Pfurtscheller, C. Brunner, A. Schlögl, and F. H. Lopes da Silva, "Mu rhythm (de)synchronization and EEG single-trial classification of different motor imagery tasks," *NeuroImage*, vol. 31, no. 1, pp. 153–159, May 2006.

[41] X. Shu, L. Yao, X. Sheng, D. Zhang, and X. Zhu, "Enhanced motor imagery-based BCI performance via tactile stimulation on unilateral hand," *Frontiers Hum. Neurosci.*, vol. 11, p. 585, Dec. 2017.

[42] M. C. Thompson, "Critiquing the concept of BCI illiteracy," *Sci. Eng. Ethics*, vol. 25, no. 4, pp. 1217–1233, Aug. 2019.

[43] Y.-F. Chen et al., "Continuous bimanual trajectory decoding of coordinated movement from EEG signals," *IEEE J. Biomed. Health Informat.*, vol. 26, no. 12, pp. 6012–6023, Dec. 2022.

[44] M. Zhang et al., "Decoding coordinated directions of bimanual movements from EEG signals," *IEEE Trans. Neural Syst. Rehabil. Eng.*, vol. 31, pp. 248–259, 2023.

[45] K. C. Ames and M. M. Churchland, "Motor cortex signals for each arm are mixed across hemispheres and neurons yet partitioned within the population response," *eLife*, vol. 8, Oct. 2019, Art. no. e46159.

[46] D. T. Bundy and E. C. Leuthardt, "The cortical physiology of ipsilateral limb movements," *Trends Neurosci.*, vol. 42, no. 11, pp. 825–839, Nov. 2019.

[47] A. R. Luft et al., "Comparing brain activation associated with isolated upper and lower limb movement across corresponding joints," *Hum. Brain Mapping*, vol. 17, no. 2, pp. 131–140, Oct. 2002.

[48] R. Zhou, L. Alvarado, R. Ogilvie, S. L. Chong, O. Shaw, and V. K. Mushahwar, "Non-gait-specific intervention for the rehabilitation of walking after SCI: Role of the arms," *J. Neurophysiol.*, vol. 119, no. 6, pp. 2194–2211, Jun. 2018.

[49] V. Dietz, "Quadrupedal coordination of bipedal gait: Implications for movement disorders," *J. Neurol.*, vol. 258, no. 8, pp. 1406–1412, Aug. 2011.

[50] S. Nakakubo, T. Doi, R. Sawa, S. Misu, K. Tsutsumimoto, and R. Ono, "Does arm swing emphasized deliberately increase the trunk stability during walking in the elderly adults?" *Gait Posture*, vol. 40, no. 4, pp. 516–520, Sep. 2014.

[51] M. F. Mridha, S. C. Das, M. M. Kabir, A. A. Lima, M. R. Islam, and Y. Watanobe, "Brain-computer interface: Advancement and challenges," *Sensors*, vol. 21, no. 17, p. 5746, Aug. 2021.

[52] H. Qiao, J. Chen, and X. Huang, "A survey of brain-inspired intelligent robots: Integration of vision, decision, motion control, and musculoskeletal systems," *IEEE Trans. Cybern.*, vol. 52, no. 10, pp. 11267–11280, Oct. 2022.